Published OnlineFirst February 15, 2011; DOI: 10.1158/0008-5472.CAN-10-0738

Cancer Research

Cooperation between *Pik3ca* and p53 Mutations in Mouse Mammary Tumor Formation

Jessica R. Adams[1,2], Keli Xu[1], Jeff C. Liu[3], Natalia M. Ruiz Agamez[1], Amanda J. Loch[1], Ruth G. Wong[1], Wei Wang[1], Katherine L. Wright[1,2], Timothy F. Lane[4], Eldad Zacksenhaus[3], and Sean E. Egan[1,2]

Abstract

PIK3CA, which codes for the p110α catalytic subunit of phosphatidylinositol 3-kinase, is one of the most frequently mutated genes in human breast cancer. Here, we describe a mouse model for *PIK3CA*-induced breast cancer by using the *ROSA26* (R26) knock-in system, in which targeted *Pik3ca* alleles can be activated through transgenic expression of Cre recombinase. We mated $Pik3ca^{H1047R}$ and $Pik3ca^{wt}$ knock-in lines with MMTV-Cre transgenics, which express Cre in mammary epithelium. Starting at approximately 5 months of age, female R26-$Pik3ca^{H1047R}$;MMTV-Cre mice, but not control R26-$Pik3ca^{wt}$;MMTV-Cre mice, developed mammary tumors, as well as lymphoid and skin malignancies. R26-$Pik3ca^{H1047R}$;MMTV-Cre mammary tumors were typically either adenosquamous carcinoma or adenomyoepithelioma. As p53 is the most commonly mutated gene in breast cancer, we tested for genetic interaction between $Pik3ca^{H1047R}$ and p53 loss-of-function mutations in R26-$Pik3ca^{H1047R}$;$p53^{loxP/+}$;MMTV-Cre mice. This led to decreased survival of double-mutant animals, which developed lymphoma and mammary tumors with rapid kinetics. Mammary tumors that formed in $p53^{loxP/+}$;MMTV-Cre conditional mutants were either poorly differentiated adenocarcinoma or spindle cell/EMT, whereas R26-$Pik3ca^{H1047R}$;$p53^{loxP/+}$;MMTV-Cre mammary tumors were mostly adenosquamous carcinoma or spindle cell/EMT indicating that double-mutant mice develop a distinct spectrum of mammary tumors. Thus, an oncogenic variant of *PIK3CA* implicated in multiple human breast cancer subtypes can induce a very diverse spectrum of mammary tumors in mice. Furthermore, $Pik3ca^{H1047R}$ shows cooperation with p53, which altered the specific tumors that formed. Thus, the two most frequently mutated genes in human breast cancer show cooperation in mammary tumor formation. *Cancer Res; 71(7); 2706–17. ©2011 AACR.*

Introduction

The phosphoinositide 3-kinase (PI3K) signaling pathway is one of the most frequently mutated pathways in cancer. One common and direct mechanism by which the PI3K pathway is activated in breast, endometrial, colorectal, urinary tract, thyroid, and ovarian cancer is through gain-of-function mutations in *PIK3CA* (1–3). *PIK3CA* mutations are particularly important in human breast cancer, with activated alleles detected in 25% to 30% of tumors (4–7). These mutations have been found in ductal carcinoma *in situ*, suggesting that they play a role in breast tumor initiation (8–10). In addition, they are present at high frequency in estrogen receptor α (ERα)-positive, Her2/Neu^{+} and triple-negative breast tumors (TNT), suggesting an important role for mutant *PIK3CA* in etiology of multiple breast tumor subtypes (4). Metaplastic breast cancers have the highest percentage of *PIK3CA* mutations (11). Importantly, *PIK3CA* mutations can induce p53-dependent growth inhibition (12) and mutations in both genes occur together in some human breast tumors (13, 14).

PIK3CA point mutations occur most often within 2 hotspots: the helix and kinase domains (1). H1047R mutations in the kinase domain account for approximately 40% of breast cancer *PIK3CA* mutant alleles (4). This mutant shows elevated kinase activity (15–17) and is capable of transforming cells in culture (18), including mammary epithelial cells (19, 20). Despite the high frequency, and hence importance of this allele in breast cancer, there is no animal model to test for its role in transformation of mammary epithelium. Here, we describe generation of a Cre-mediated system to conditionally express *Pik3ca* alleles in mouse tissues, and use of this system to test for induction of mammary tumor formation by $Pik3ca^{H1047R}$. We report that ectopic expression of $Pik3ca^{H1047R}$, but not $Pik3ca^{wt}$, induced mammary tumors at high frequency. Furthermore, we have used the knock-in system to test for

Authors' Affiliations: [1]Program in Developmental and Stem Cell Biology, The Hospital for Sick Children; [2]Department of Molecular Genetics, University of Toronto; and [3]Division of Cell & Molecular Biology, Toronto General Research Institute—University Health Network, Toronto, Ontario, Canada; and [4]Jonsson Comprehensive Cancer Center, Department of Obstetrics and Gynecology and Department of Biological Chemistry, David Geffen School of Medicine, University of California, Los Angeles, Los Angeles, California

Note: Supplementary material for this article is available at Cancer Research Online (http://cancerres.aacrjournals.org/).

Corresponding Author: Sean E. Egan, The Hospital for Sick Children, 101 College Street, TMDT, #14-309, Toronto, Ontario, Canada M5G-1L7. Phone: 416-813-5267; Fax: 416-813-5252; E-mail: segan@sickkids.ca

doi: 10.1158/0008-5472.CAN-10-0738

Published OnlineFirst February 15, 2011; DOI: 10.1158/0008-5472.CAN-10-0738

cooperation between *Pik3ca* and p53 (3), showing that deletion of p53 enhances tumor formation and alters the spectrum of mammary tumor subtypes that form in our *Pik3ca*^{H1047R} model.

Materials and Methods

Generation of transgenic mice

Shuttle vectors containing either wild-type or H1047R mutant *Pik3ca* were subcloned into the pROSA26PA gene-targeting vector (21, 22). pR26-Pik3ca plasmids were linearized with *Kpn*I (Fig. 1) and electroporated into mouse embryonic stem cells (mESC). G418-resistant clones were isolated, expanded, and screened by Southern blot (probing for the 3′ recombination junction—see following text) and PCR [amplifying across the 5′ recombination junction, forward primer (FP) 5′-CGCCTAAAGAAGAGGCTGTG-3′, reverse primer (RP) 5′-GAAAGACCGCGAAGAGTTTG-3′]. Targeted clones were transiently transfected (Fugene6, Roche 11815091001) with Cre or control vector (pCAGGS-Cre-IRES-puro; pCAGGS-FlpE-IRES-puro; ref. 23). RNA was harvested (RNeasy, Qiagen 74104) and RT-PCR performed (SuperScript II, Invitrogen 18064022) by using FP in R26 exon 1 (5′-CTAGGTAGGGGATCGGGACTCT-3′) and a RP in *Pik3ca* cDNA (5′-AATTTCTCGATTGAGGATCTTTTCT-3′). Cre-inducible mESC lines were used for morula aggregation in the Toronto Centre for Phenogenomics (TCP).

Southern blot analysis

A standard Southern blot protocol was used. Genomic DNA (10 μg) was digested with *Eco*RV/*Sst*I. An approximately 940 bp probe on the 3′ side of the targeted insertion site (CTTGAAAGTGGAGTAACTAC to TCAGAAGCTTTGAACTAGAA in the R26 locus) was ^{32}P-labeled, using the Random Primers DNA Labeling System (Invitrogen 18187013). This probe binds an 11 kb fragment in nontargeted R26, and a 9 kb fragment if the R26 locus is correctly targeted.

Mouse colony maintenance

Mice were housed at TCP according to guidelines from the Canadian Council on Animal Care (CCAC). Cre strains were genotyped by using FP 5′-TCGCGATTATCTTCTATATCTTCAG-3′, RP 5′-GCTCGACCAGTTTAGTTACCC-3′. R26-Pik3ca mice were genotyped by using primers previously published (22). Multiparous females had 3 litters. p53$^{loxP/+}$ conditional mutant mice (FVB.129-*Trp53*^{tm1Brn}–MMHCC 01XC2; for simplicity, this strain is labeled throughout as p53$^{f/+}$; ref. 24) were obtained from the Mouse Models of Human Cancer Consortium and genotyped by PCR (FP 5′-CACAAAAACAGGTTAAACCCAG-′, RP 5′-AGCACATAGGAGGCAGAGAC-3′). p53 deletion was confirmed by using FP 5′-CACAAAAACAGGTTAAACCCAG-3′, RP 5′-GAAGACAGAAAAGGGGAGGG-3′ to amplify a 612 bp fragment (24).

RT-PCR on lin$^-$ mammary epithelium

Mammary glands from young virgin mice were minced and digested in collagenase/hyaluronidase (Stem Cell Technologies 07912) for 4 hours (37°C). Mammary epithelial (lineage-depleted; lin$^-$) cells were isolated by using the EasySep kit (StemCell Technologies 19757). RT-PCR was performed as outlined earlier in the text.

Tumor collection

Mice were humanely sacrificed at endpoint, and mammary tumors dissected. Humane endpoint was based on criteria outlined by the CCAC (tumor volume = 1.7 cm^3, tumor mass = 5% of body weight, or ulcerated tumor). Part of each tumor was fixed in 10% formalin and embedded in paraffin. The remaining tumor was divided into small samples and snap frozen.

Western blots

Tumors and control glands were lysed by using a TissueRuptor homogenizer (Qiagen 9001271) in lysis buffer (ProteoJET Lysis Reagent, Fermentas K0301; PhosSTOP, Roche 04906837001; protease inhibitor, Roche 11836170001). Protein lysates (150 μg) were analyzed using a standard Western blot protocol. Primary antibodies were incubated overnight and secondary antibodies for 1 hour, both at room temperature. Western blots were quantified using AlphaImager software (Cell Biosciences) and normalized with respect to β-actin expression. Antibodies (used at recommended dilutions) are as follows: Akt^{pT308} (Cell Signaling CS2965), Akt^{pS473} (Cell Signaling CS927), PTEN (Cell Signaling CS9559), c-Jun^{pS73} (Cell Signaling CS3270), SGK3^{pS486} (SantaCruz sc33044), ERα (SantaCruz sc71064), Atf3 (SantaCruz sc188), β-catenin (BDTL 610154), carbonic anhydrase IX (CAIX; R&D Systems AF2344), β-actin (abCam ab8226), goat anti-rabbit IgG-HRP (SantaCruz sc2004), goat anti-mouse IgG-HRP (SantaCruz sc2005), donkey anti-goat IgG-HRP (SantaCruz sc2020).

Histology and immunohistochemistry

Five-micrometer paraffin sections were either stained with hematoxylin and eosin, or subjected to antigen retrieval in a decloaking chamber (Biocare Medical; SetPoint1 = 125°C, 5 minutes; SetPoint2 = 90°C, 10 seconds), using epitope-retrieval solution (Biocare Medical BD1000G1 or RV1000G1). Slides were mounted into a Tecan FreedomEvo liquid-handling robot.

Immunohistochemistry: endogenous peroxidases were quenched in 3% H_2O_2/methanol (15 minutes, room temperature), then VectaStain ABC kits (Vector Laboratories) were used (PK-6101, PK-4002, PK-6105). Antibodies were incubated for 30 minutes at room temperature. 3,3′-Diaminobenzidine (DAB) substrate kit (Vector Laboratories SK-4100) was used for staining and slides were counterstained in hematoxylin (10 seconds).

Immunofluorescence: slides were blocked for 30 minutes (DakoCytomation X0909). Primary antibodies were incubated overnight (4°C), secondary antibodies were incubated for 1 hour (room temperature). Slides were mounted with fluorescence mounting medium (DakoCytomation S3023) containing 4′,6-diamidino-2-phenylindole (DAPI).

Antibodies (used at recommended dilutions) are as follows: Gata3 (ProteinTech 10417–1-AP), Cytokeratin 5 (Covance

Published OnlineFirst February 15, 2011; DOI: 10.1158/0008-5472.CAN-10-0738

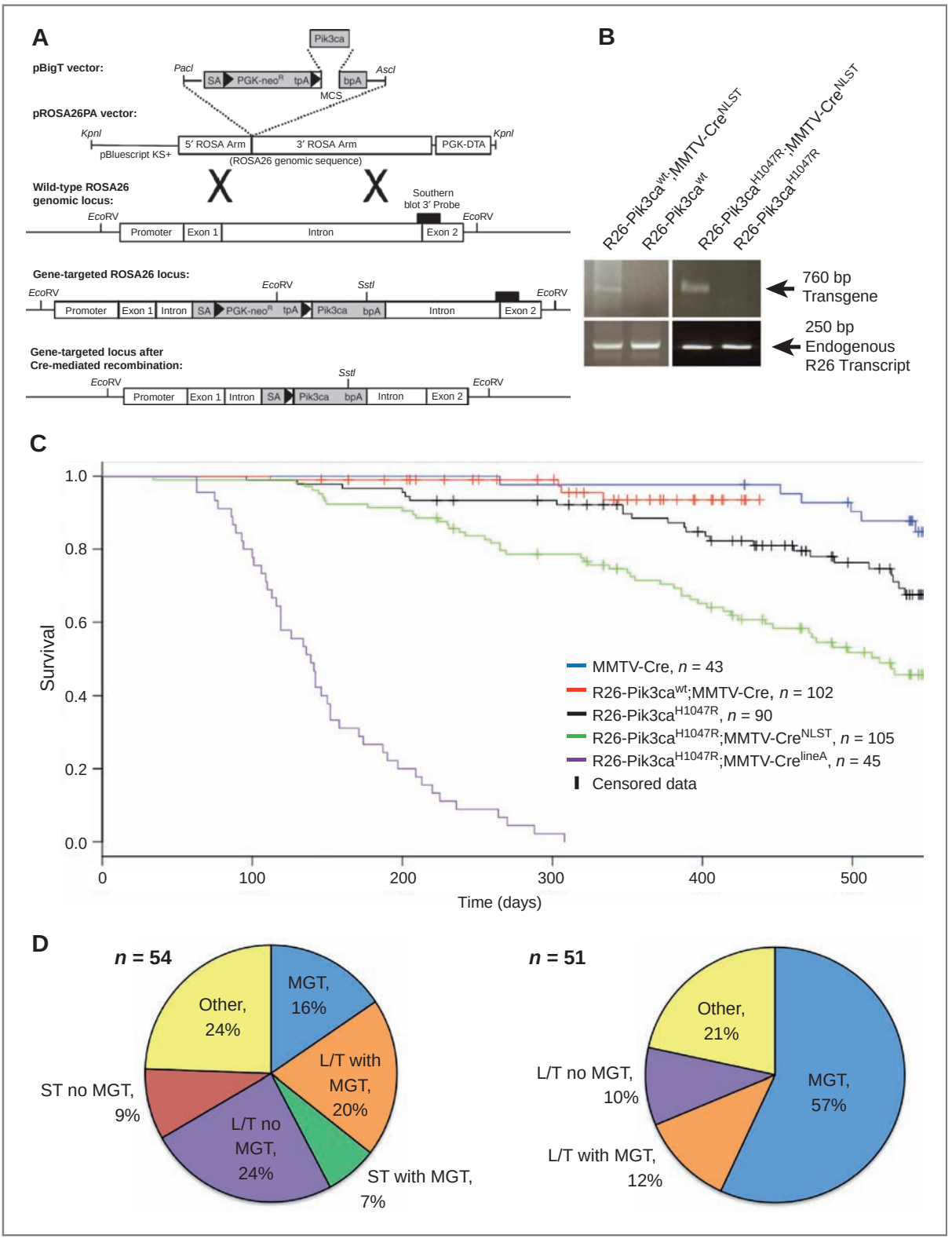

Figure 1. R26-Pik3ca^{H1047R};MMTV-Cre mice develop tumors in the mammary gland, skin, and lymphocytic tissue. A, conditional knock-in mice were generated by recombining mouse *Pik3ca* cDNAs (preceded by a loxP-flanked transcriptional stop cassette) into the R26 locus (22). B, lin$^-$ mammary epithelium from R26-Pik3ca;MMTV-Cre mice expressed their respective transgene, whereas cells from Cre$^-$ littermates did not. C, Kaplan–Meier survival curves for R26-Pik3ca^{H1047R};MMTV-Cre female mice. D, cause of death data for R26-Pik3ca^{H1047R};MMTV-Cre^{lineA} (left) and R26-Pik3ca^{H1047R};MMTV-Cre^{NLST} (right) mice. "Other" includes mice that died without obvious tumors (e.g., with dystocia) or mice that could not be examined because of decomposition. MGT, mammary gland tumors; L/T, lymphoma/thymoma; ST, skin tumors.

Published OnlineFirst February 15, 2011; DOI: 10.1158/0008-5472.CAN-10-0738

PRB-160P), ERα (SantaCruz sc542), Ki67 (BioCare Medical CRM326), Cytokeratin 8 (Fitzgerald 10R-C177AX), Cytokeratin 14 (Panomics E2624), Cytokeratin 10 (Covance PRB-159P), vimentin (Vim; SantaCruz sc32322), desmin (Des; DakoCytomation M0760), N-cadherin (N-Cad; Novus NB200–592), AlexaFluor488 anti-mouse (Invitrogen A21202), AlexaFluor594 anti-rabbit (Invitrogen A21442).

TUNEL

Five-micrometer paraffin sections were immersed in 2.5 μg/mL proteinaseK (2 minutes). Endogenous peroxidases were quenched via 3% H_2O_2 (15 minutes). Terminal deoxynucleotidyl transferase-mediated dUTP nick end labeling (TUNEL) was performed by using terminal deoxynucleotidyl transferase (Fermentas EP0161) and biotin-16-UTP (Roche 11093070910). Signal was amplified (ABC, Vector Laboratories PK-6100) and developed (DAB Kit, Vector Laboratories SK-4100); sections were counterstained with methyl green.

Image capture

Images were captured with an AxioCam HRm digital camera (Zeiss) by using AxioVision (release 4.6.3) software.

Results

Generation of a Cre-inducible *Pik3ca* mammary tumor model

To test for the ability of *Pik3ca*^{H1047R} or wild-type *Pik3ca* (*Pik3ca*^{wt}) to induce mammary tumors, we used the Cre-conditional *ROSA26* (R26) knock-in system, whereby Cre-mediated deletion of loxP-flanked transcriptional stop sequences allows for tissue-specific expression of either allele (Fig. 1A; refs. 21, 22). mESC were targeted and screened to identify clones with Cre-inducible transgene expression (Supplementary Fig. 1). Cre-responsive mESC clones were then used to generate chimeric mice, and germline transmission of each knock-in allele confirmed. R26-Pik3ca^{H1047R} and R26-Pik3ca^{wt} mice were mated with MMTV-Cre mice, which express Cre-recombinase in mammary epithelium. Two different strains of MMTV-Cre were used: MMTV-Cre^{lineA}, which expresses Cre recombinase in mammary epithelium at high efficiency and also in skin and lymphocytes (25); MMTV-Cre^{NLST}, which is less efficient but more mammary restricted in its expression (Supplementary Fig. 2; refs. 26, 27). Mammary-inducible transgene expression was observed in R26-Pik3ca;MMTV-Cre mice but not in Cre-negative littermates (Fig. 1B).

Female R26-Pik3ca^{H1047R};MMTV-Cre mice from both Cre lines showed reduced survival (Fig. 1C; Supplementary Table 1; note, males were not studied). Some animals died abruptly, whereas most were sacrificed at humane endpoint due to lethargy and impaired breathing or solid tumor growth. Decreased survival was not because of *Pik3ca* overexpression as R26-Pik3ca^{wt};MMTV-Cre mice remained healthy (Fig. 1C). R26-Pik3ca^{H1047R};MMTV-Cre mice started developing mammary tumors at 5 months of age. Mammary tumors were observed in both virgin and multiparous mice using either MMTV-Cre strain. R26-Pik3ca^{H1047R};MMTV-Cre^{lineA} mice reached endpoint more rapidly than R26-Pik3ca^{H1047R};MMTV-Cre^{NLST} mice (Fig. 1C). In addition, R26-Pik3ca^{H1047R};MMTV-Cre^{lineA} mice reached endpoint with a more diverse set of tumor types. 69% of NLST mice and 42% of line A mice and had palpable mammary tumors at endpoint (Fig. 1D). For this reason, we used MMTV-Cre^{NLST} transgenics for subsequent studies. Development of lymphoma/thymoma, skin, and other nonmammary tumors was attributed to Cre expression in other tissues (25). Interestingly, survival of R26-Pik3ca^{H1047R} mice, without Cre, was reduced in comparison with MMTV-Cre controls (Fig. 1C; Supplementary Table 1; $P < 1\times10^{-6}$). This was due to development of blood vessel lesions in some R26-Pik3ca^{H1047R} animals (data not shown), potentially through spontaneous activation of *Pik3ca*^{H1047R} expression in endothelial cells (28).

Pik3ca and p53 mutations cooperate *in vivo*

To test for cooperation between *Pik3ca* and p53, we mated R26-Pik3ca^{H1047R};MMTV-Cre^{NLST} mice with Cre-conditional p53 mutants (24). Most R26-Pik3ca^{H1047R};p53$^{f/f}$;MMTV-Cre^{NLST} mice died early with lymphoma/thymoma (Fig. 2A). On autopsy, some had small mammary tumors (Fig. 2C, left). Lymphoma/thymoma occurred at a much lower rate in R26-Pik3ca^{H1047R};p53$^{f/+}$;MMTV-Cre^{NLST} p53 heterozygous mice, which also showed significantly reduced survival as compared with R26-Pik3ca^{H1047R};MMTV-Cre^{NLST}, p53$^{f/+}$;MMTV-Cre^{NLST}, and Cre-negative control mice (Fig. 2A; Supplementary Table 2). To test whether *Pik3ca* and p53 show an additive or synergistic interaction, we simulated a Kaplan–Meier survival curve by combining single-mutant cohorts, such that as any R26-Pik3ca^{H1047R};MMTV-Cre^{NLST} or p53$^{f/+}$;MMTV-Cre^{NLST} mouse reached endpoint, it was scored as an event within one cohort. R26-Pik3ca^{H1047R};p53$^{f/+}$;MMTV-Cre^{NLST} double-mutant mice showed significantly decreased survival ($P = 2.79\times10^{-5}$) compared with this hypothetical cohort indicating synergy between *Pik3ca*^{H1047R} and p53 gene loss. Synergistic interaction was also evident when considering only mice that reached endpoint from mammary tumors (Supplementary Fig. 3). p53 deletion was observed in R26-Pik3ca^{H1047R};p53$^{f/+}$;MMTV-Cre^{NLST} and p53$^{f/+}$;MMTV-Cre^{NLST} tumors (Fig. 2B). Ninety-two percent of p53$^{f/+}$;MMTV-Cre^{NLST} and 80% of R26-Pik3ca^{H1047R};p53$^{f/+}$;MMTV-Cre^{NLST} mice had mammary tumors (Fig. 2C). Many mice had mammary tumors in more than one gland. These were treated as distinct lesions.

Histologic analysis revealed that mammary tumors from R26-Pik3ca^{H1047R};MMTV-Cre^{NLST} mice were typically either adenosquamous carcinoma or adenomyoepithioma (Fig. 3A; Supplementary Fig. 4). Adenosquamous tumors contained cystic regions composed of laminar keratin lined with squamous epithelium and adjacent glandular elements. Some tumors had squamous nodules or necrosis, and several had invasive margins. Expansile tumors were also observed. Adenomyoepitheliomas contained a mixture of glandular epithelium and interstitial fusiform cells with abundant polar cytoplasm. These myoepithelial stromal cells represented 10% to 80% of the tumor. Isolated lung metastasis were

Published OnlineFirst February 15, 2011; DOI: 10.1158/0008-5472.CAN-10-0738

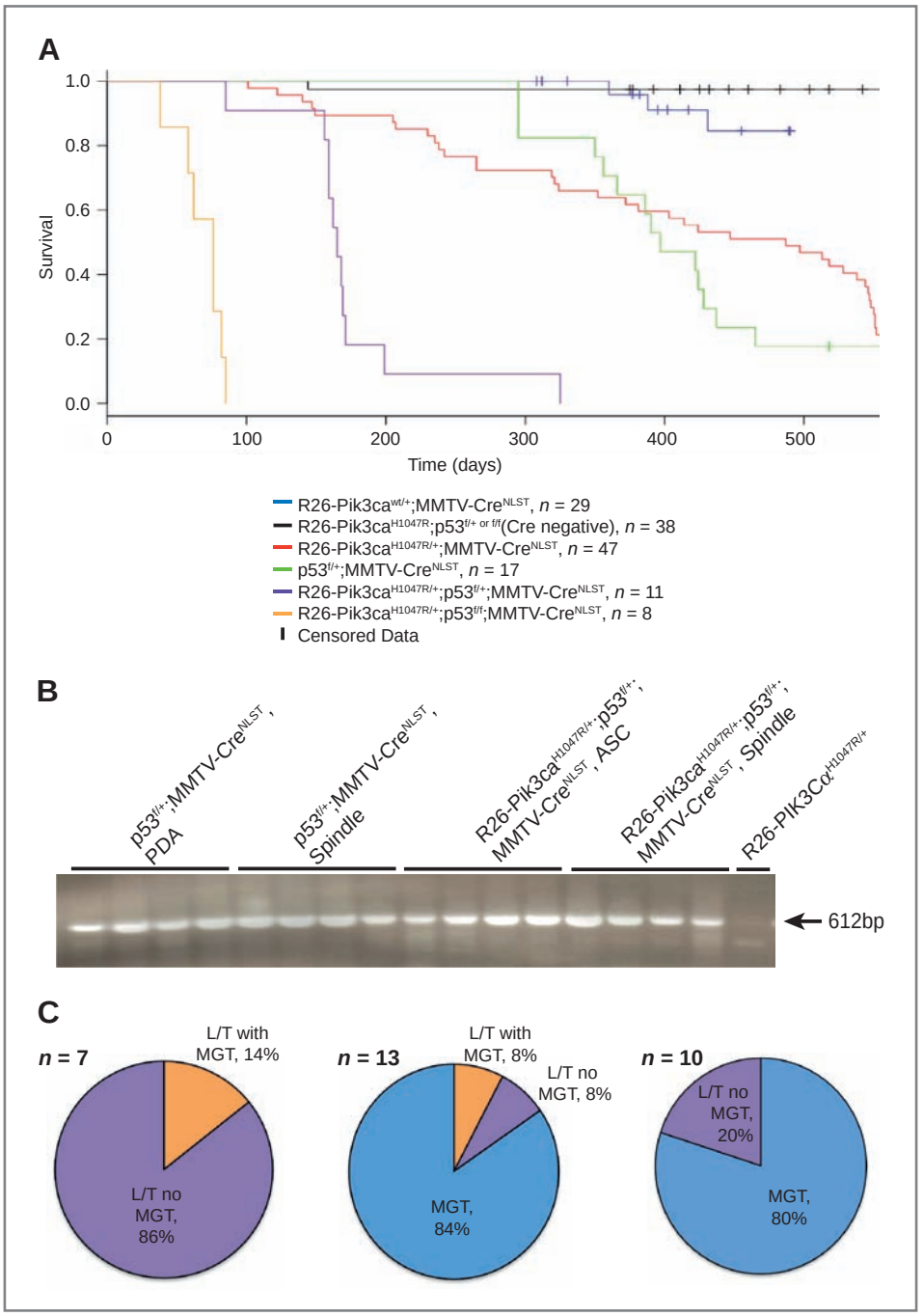

Figure 2. *Pik3ca^{H1047R}* and p53 deletion show cooperation in mice. A, Kaplan–Meier survival curves. B, p53 deletion in tumor DNA was confirmed via PCR (diagnostic 612bp fragment). C, cause of death data for R26-Pik3ca^{H1047R};p53$^{f/f}$;MMTV-Cre^{NLST} (left), p53$^{f/+}$;MMTV-Cre^{NLST} (middle), and R26-Pik3ca^{H1047R};p53$^{f/+}$;MMTV-Cre^{NLST} (right) mice.

observed in rare R26-Pik3ca^{H1047R};MMTV-Cre^{NLST} mice (data not shown). Mammary tumors from p53$^{f/+}$;MMTV-Cre^{NLST} mice were either spindle/epithelial-mesenchymal transition (EMT) type or poorly differentiated adenocarcinoma as previously reported (Fig. 3B; Supplementary Fig. 4; refs. 29–31). Spindle tumor cells had fusiform nuclei and polar cytoplasm. Swirling patterns and necrotic areas were observed. Poorly differentiated adenocarcinomas were composed of solid sheets of cells with little tissue architecture and some necrosis. Cells had large, pleomorphic nuclei and dark staining cytoplasm. Interestingly, mammary tumors that formed in R26-Pik3ca^{H1047R};p53$^{f/+}$;MMTV-Cre^{NLST} double-mutant mice were typically either spindle/EMT or adenosquamous carcinoma (Fig. 3C; Supplementary Fig. 4). Radial scar and poorly differentiated adenocarcinomas were also observed, although at a lower frequency (Fig. 3C; Supplementary Fig. 4). Radial scar tumors were small and had a stellate outline composed of dense connective tissue and a center with distorted neoplastic glands. Gross metastasic lesions were not observed in R26-Pik3ca^{H1047R};p53$^{f/+}$;MMTV-Cre^{NLST} mice (data not shown).

Published OnlineFirst February 15, 2011; DOI: 10.1158/0008-5472.CAN-10-0738

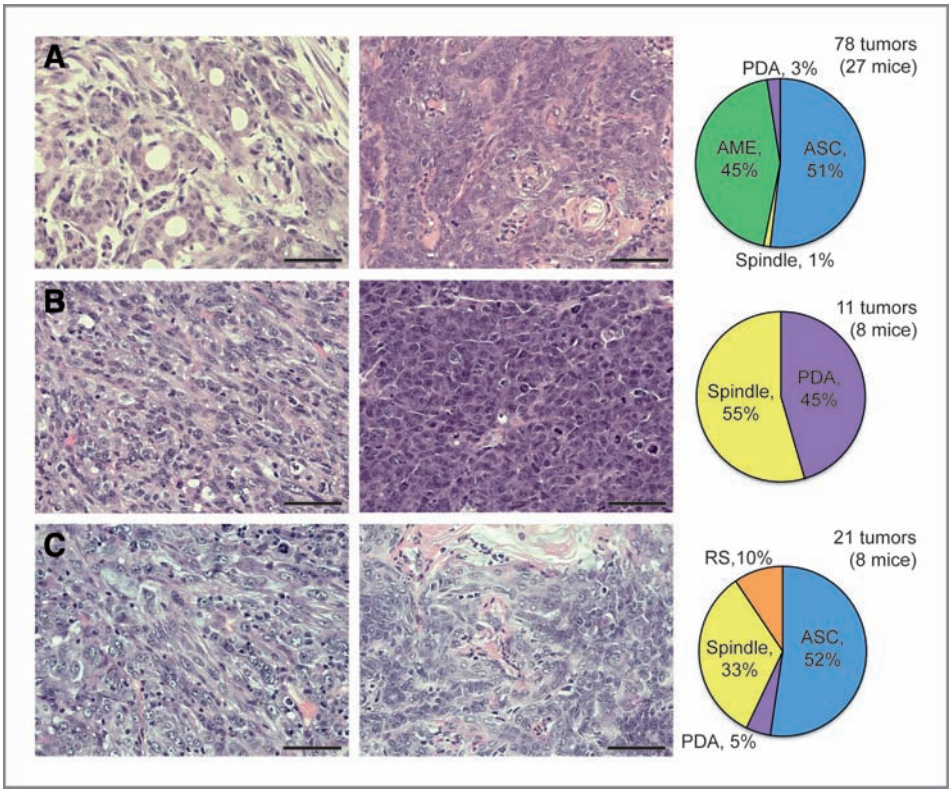

Figure 3. Mammary tumor pathology in R26-Pik3ca^{H1047R};p53^{f};MMTV-Cre^{NLST} mice. A, mammary tumors in R26-Pik3ca^{H1047R};MMTV-Cre^{NLST} mice are mostly adenomyoepitheliomas (AME; left) or adenosquamous carcinomas (ASC; middle). B, p53$^{f/+}$;MMTV-Cre^{NLST} mice develop mammary spindle cell tumors (left) or poorly differentiated adenocarcinomas (PDA; middle). C, R26-Pik3ca^{H1047R};p53$^{f/+}$;MMTV-Cre^{NLST} mice develop mostly spindle cell tumors (left) or ASCs (middle). Some developed radial scar (RS) or PDAs (right). Scale bars, 50 μm.

Akt activation in *Pik3ca^{H1047R}* and p53 mutant mammary tumors

To test for PI3K pathway activation, lysates from representative tumors were analyzed for Akt phosphorylation, and for expression of PTEN and phospho-c-Jun (S73). Western blot signals were normalized to β-actin protein expression, and compared with levels in mammary lysates from a non–tumor-bearing 74-week-old R26-Pik3ca^{H1047R} virgin female. Adenosquamous carcinomas from R26-Pik3ca^{H1047R};MMTV-Cre^{NLST} mice showed elevated accumulation of phospho-Akt^{S473}, PTEN, and phospho-c-Jun^{S73} (Fig. 4). Adenosquamous carcinomas from R26-Pik3ca^{H1047R};p53$^{f/+}$;MMTV-Cre^{NLST} showed increased PTEN and phospho-c-Jun^{S73} expression. Surprisingly, however, no change in phospho-Akt was observed in these tumors. The reason for this is not clear, perhaps representing a change in PI3K signaling such as a reduced dependence on Akt activation (32). Alternatively, the wild-type sample used for normalization in this experiment was whole mammary gland lysate. This tissue contains a large amount of insulin-responsive fat, and may show higher basal levels of Akt activation than mammary epithelium. We therefore tested additional adenosquamous tumors from R26-Pik3ca^{H1047R};MMTV-Cre mice for phospho-Akt and used lin^{-} mammary epithelium as control. Indeed, phospho-Akt^{T308} and phospho-Akt^{S473} were significantly elevated in 12 adenosquamous carcinomas from R26-Pik3ca^{H1047R};MMTV-Cre mice (Supplementary Fig. 5).

Elevated levels of phospho-Akt^{T308} and phospho-Akt^{S473} were observed in lysates from adenomyoepithelioma lesions in R26-Pik3ca^{H1047R};MMTV-Cre^{NLST} mice and in lysates from R26-Pik3ca^{H1047R};p53$^{f/+}$;MMTV-Cre^{NLST} spindle/EMT tumors. Interestingly, elevated levels of phospho-Akt^{T308} and phospho-Akt^{S473} were also seen in lysates from spindle/EMT and in poorly differentiated adenocarcinomas from p53$^{f/+}$;MMTV-Cre^{NLST} mice. Elevated levels of PTEN expression and of phospho-c-Jun accumulation were observed in each mammary tumor type studied. In the case of PTEN, this is likely a result of PI3K pathway–induced phosphorylation and stabilization of PTEN, a negative feedback loop which functions to decrease PIP_3 levels (33). Also, increased phospho-c-Jun is associated with elevated PI3K pathway activation (34). Finally, it has been suggested that activation of other PDK1 substrate kinases, such as SGK3, may play an important role downstream of *PIK3CA* gene mutation in breast cancer (32). We therefore analyzed SGK3 phosphorylation in these tumors. Phospho-SGK3^{S486} was not elevated in any of the tumor types analyzed (Supplementary Fig. 6).

Pik3ca^{H1047R} mice form multiple mammary tumor subtypes

PIK3CA gene mutations are found in ERα-positive, HER2/Neu-positive, and TNT cancers (4–7). To further define mammary tumor subtype in our *Pik3ca* model, we stained representative tumors for expression of luminal and basal cell cytokeratin, cytokeratin 8 (K8) and cytokeratin 14 (K14), respectively (Fig. 5; Supplementary Fig. 7). Glandular regions of R26-Pik3ca^{H1047R};MMTV-Cre^{NLST} adenosquamous carcinomas contained cells expressing either cytokeratin. Mammary architecture was maintained in glandular regions, in that K14^{+} cells surrounded layers of K8^{+} cells (Fig. 5A, middle).

Published OnlineFirst February 15, 2011; DOI: 10.1158/0008-5472.CAN-10-0738

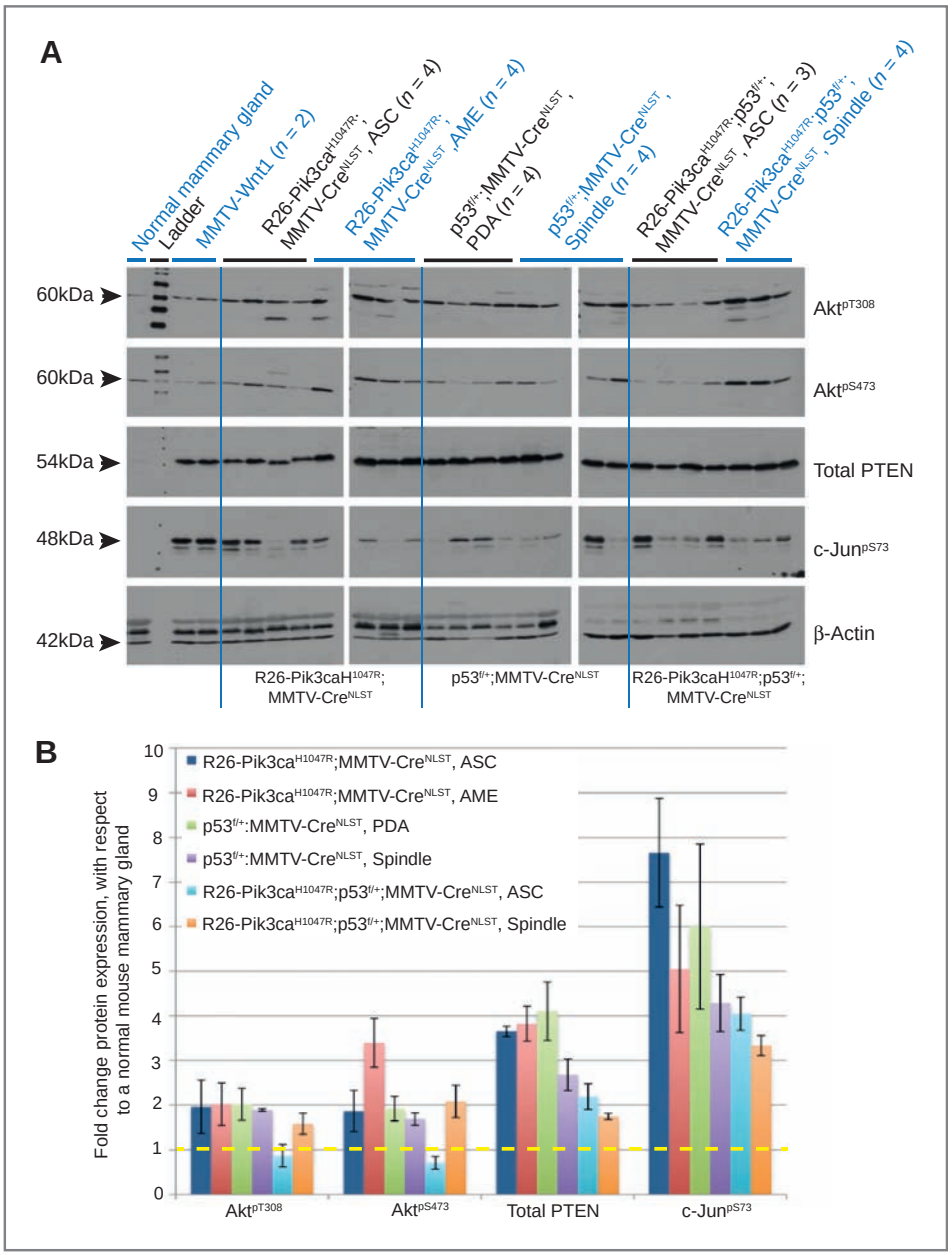

Figure 4. Akt activation in mammary tumors from *Pik3ca*^{H1047R} model mice. A, Western blot analysis of PI3K-pathway components and phospho-c-Jun. B, Western blot signals were quantified and normalized with respect to β-actin. Mean fold increase compared with mammary lysate from a control mouse was calculated after normalization. Bars, group mean values; error bars, ±SE; asterisks, significant increase in expression (1-sided 1-sample *t* test; $\alpha = 0.05$; *, $P < 0.05$ and **, $P < 0.1$). Yellow dashed line, protein expression in a normal mammary gland.

K8$^+$ cells in these regions also expressed Gata3, albeit at a level lower than in adjacent normal glands (data not shown; ref. 35). The glandular epithelium in R26-Pik3ca^{H1047R};MMTV-Cre^{NLST} adenomyoepitheliomas also stained positive for both cytokeratin (Fig. 5A, right). K14$^+$ expression was noted in interstitial fusiform cells surrounding glandular type structures (data not shown). Spindle tumors from p53$^{f/+}$;MMTV-Cre^{NLST} mice had few K8- or K14-positive cells (Fig. 5B, left). In contrast, cells in poorly differentiated adenocarcinomas from p53$^{f/+}$;MMTV-Cre^{NLST} mice were mostly either K14$^+$ (Fig. 5B, middle) or K8$^+$ (Fig. 5B, right). Some double-negative regions and regions with double-positive cells were also observed (data not shown). Adenosquamous carcinomas from R26-Pik3ca^{H1047R};MMTV-Cre^{NLST} and R26-Pik3ca^{H1047R};p53$^{f/+}$;MMTV-Cre^{NLST} mice showed the same staining pattern (Fig. 5C, left). Similarly, K14 and K8 staining in spindle/EMT (Fig. 5C, middle) and poorly differentiated adenocarcinomas (Fig. 5C, right) from R26-Pik3ca^{H1047R};p53$^{f/+}$;MMTV-Cre^{NLST} and p53$^{f/+}$;MMTV-Cre^{NLST} mice was indistinguishable (note, right panel of Fig. 5C shows a tumor region with many K14$^+$/K8$^+$ double-positive cells; such regions were also frequently observed in poorly differentiated adenocarcinomas from p53$^{f/+}$;MMTV-Cre^{NLST} mice as described earlier). K5 immunostaining closely matched with that observed for K14 in each case (data not shown).

ERα expression was noted in R26-Pik3ca^{H1047R};MMTV-Cre^{NLST} (Fig. 5D) and R26-Pik3ca^{H1047R};p53$^{f/+}$;MMTV-Cre^{NLST}

Published OnlineFirst February 15, 2011; DOI: 10.1158/0008-5472.CAN-10-0738

(data not shown) adenosquamous carcinomas, although nuclear staining appeared reduced in most tumor cells as compared with that observed in normal ducts (Fig. 5D, inset). R26-Pik3ca^{H1047R};MMTV-Cre^{NLST} adenomyoepitheliomas also contained nuclear ERα^{+} cells (Fig. 5D, right). In contrast, less signal was observed in other tumor types. To better quantify ERα expression, Western blot analysis was performed on tumor lysates (Fig. 5D, bottom). Adenosquamous carcinomas (from R26-Pik3ca^{H1047R};MMTV-Cre^{NLST} and R26-Pik3ca^{H1047R};p53$^{f/+}$;MMTV-Cre^{NLST}) as well as adenomyoepitheliomas from R26-Pik3ca^{H1047R};MMTV-Cre^{NLST} mice expressed similar levels of ERα as in the control gland. In contrast, ERα expression was decreased in p53$^{f/+}$;MMTV-Cre^{NLST} poorly differentiated carcinomas, R26-Pik3ca^{H1047R};p53$^{f/+}$;MMTV-Cre^{NLST} spindle/EMT tumors and trended toward decreased expression in p53$^{f/+}$;MMTV-Cre^{NLST} spindle/EMT tumors (Fig. 5D).

Next, we stained for the EMT marker N-Cad and, in some tumors, for Des or Vim (Fig. 6; Supplementary Fig. 8; refs. 27, 36, 37). R26-Pik3ca^{H1047R};MMTV-Cre^{NLST} adenosquamous carcinomas had scattered N-Cad^{+} cells and Vim^{+} cells in squamous regions (Fig. 6A). R26-Pik3ca^{H1047R};MMTV-Cre^{NLST} adenomyoepitheliomas had many N-Cad^{+} cells and some Des^{+} cells in nonglandular regions (Fig. 6B). In contrast, N-Cad^{+} cells were observed throughout spindle/EMT tumors from p53$^{f/+}$;MMTV-Cre^{NLST} and R26-Pik3ca^{H1047R};p53$^{f/+}$;MMTV-Cre^{NLST} mice (Fig. 6C, left). Both also had rare Des^{+} cells. Adenosquamous carcinomas from R26-Pik3ca^{H1047R};p53$^{f/+}$;MMTV-Cre^{NLST} animals had some N-Cad^{+}, but no Des^{+} cells. Finally, poorly differentiated adenocarcinomas from p53$^{f/+}$;MMTV-Cre^{NLST} mice showed no evidence of EMT. Adenosquamous carcinomas from R26-Pik3ca^{H1047R};MMTV-Cre^{NLST} single or Pik3ca^{H1047R};p53$^{f/+}$;MMTV-Cre^{NLST} double-mutant mice also contained cells expressing a marker of differentiated squamous epithelium, cytokeratin 10 (K10). K10^{+} cells were typically found lining keratinized cysts (Fig. 6C, right; Supplementary Fig. 8). Atf3 has been implicated in squamous cell carcinoma (38) and accumulated to widely variable levels in our mammary tumors. For example, some R26-Pik3ca^{H1047R};MMTV-Cre^{NLST} tumors (adenosquamous carcinomas and adenomyoepitheliomas) and some p53$^{f/+}$;MMTV-Cre^{NLST} poorly differentiated carcinomas expressed Atf3. Expression was not observed in other tumor types (Supplementary Fig. 9). Mammary tumors of all genotypes appeared less bloody than MMTV-Wnt1 control tumors. This was typically associated with less vasculature and, in most cases, with elevated expression of carbonic anhydrase CAIX, an indirect marker of hypoxia (Supplementary Fig. 9; ref. 39). Interestingly, elevated β-catenin levels, comparable with levels in MMTV-Wnt1 tumors, were observed in both major tumor types from R26-Pik3ca^{H1047R};MMTV-Cre^{NLST} mice and in poorly differentiated adenocarcinomas in p53$^{f/+}$;MMTV-Cre^{NLST} mice, suggesting that Wnt signaling may be activated in each case (Supplementary Fig. 9).

To quantify cell proliferation and apoptosis in each tumor type, we performed Ki67 immunohistochemistry and TUNEL analysis, respectively (Table 1; Supplementary Table 3). Each tumor type examined had very low levels of TUNEL-positive nuclei (<1% in all cases). This result is not surprising given that PI3K pathway activation and p53 gene deletion are both associated with enhanced cell survival. In contrast, the percentage of Ki67-positive nuclei varied with genotype and tumor type. Mammary tumors from R26-Pik3ca^{H1047R};MMTV-Cre^{NLST} mice had the highest proportion of Ki67-positive nuclei, whereas p53$^{f/+}$;MMTV-Cre^{NLST} tumors had the lowest. In tumor type analysis, adenosquamous carcinomas had the highest Ki67 index whereas poorly differentiated carcinomas had the lowest.

Discussion

PIK3CA is commonly mutated in human breast cancer. The *PIK3CA* locus is also amplified in some breast cancers (6, 40, 41). To test for initiation of mammary tumor formation by *PIK3CA* alleles we generated syngeneic R26-Pik3ca^{H1047R} and R26-Pik3ca^{wt} knock-in mice. Each strain carried a Cre-inducible allele of mouse *Pik3ca*, and each was crossed to MMTV-Cre mice to activate expression within mammary epithelium. Starting at 5 months, R26-Pik3ca^{H1047R};MMTV-Cre females developed mammary tumors at a high frequency. Importantly, R26-Pik3ca^{wt};MMTV-Cre mice did not. Thus, low-level ectopic expression of p110α^{H1047R}, but not p110α^{wt}, is sufficient to initiate mammary tumor formation in mice. This result is consistent with identification of H1047R mutations in premalignant lesions (8–10). We did not observe any gross abnormalities in glands of young R26-Pik3ca^{H1047R};MMTV-Cre^{NLST} mice, likely because of inefficient Cre-deletion in this line. It will be important to define early responses to PIK3CA^{H1047R} gene activation in our model, perhaps using line A or through *ex vivo*, Cre-induced, gene activation and transplantation.

PIK3CA mutations occur in all major subtypes of human breast cancer (4–7, 11). Our mouse model of *Pik3ca^{H1047R}*-induced breast cancer develops adenosquamous carcinoma and adenomyoepithelioma of the mammary gland at high frequency. Both tumor types were ERα^{+}. Both also contained luminal and myoepithelial keratin-positive cells, suggesting that the cell of origin had bilineage potential. As *PIK3CA* and *TP53* are the 2 most commonly mutated genes in human breast cancer, and mutations in both occur together in many tumors, we tested for cooperation between these genes in our model. Indeed, we observed reduced survival of R26-Pik3ca^{H1047R};p53^{f};MMTV-Cre^{NLST} double-mutant animals. Cooperation between *Pik3ca^{H1047R}* and p53 loss-of-function mutation is in contrast to the situation observed in MMTV-myrPik3ca mice, in which mammary tumor formation is enhanced by expression of CDK4^{R24C} but not by deletion of one p53 allele (42). In our model, apoptosis was very low in all of the tumors analyzed. In contrast, the proliferation rate varied significantly from one tumor type to another, tracking more closely with tumor type than with genotype. Thus, the observed cooperation between *pik3ca^{H1047R}* and p53 loss-of-function mutation is not at the level of apoptosis or proliferation. Indeed, data presented in Figures 2A and 3C indicate that *pik3ca^{H1047R}* and p53 mutations cooperate in mammary tumor initiation and interact to control mammary tumor type. In total, on wild-type and p53 mutant backgrounds, we observed

Published OnlineFirst February 15, 2011; DOI: 10.1158/0008-5472.CAN-10-0738

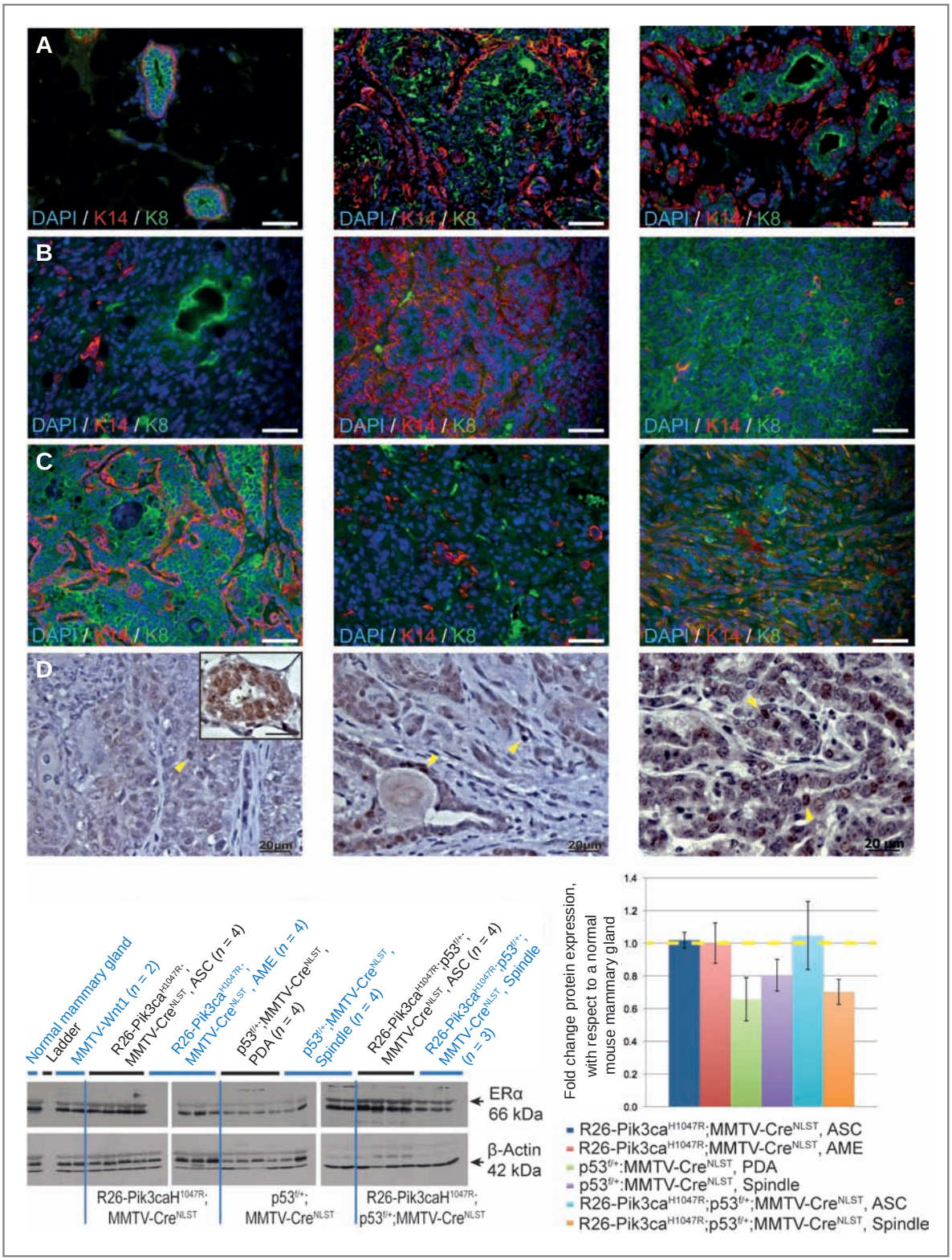

Figure 5. Expression of luminal and basal differentiation markers and ERα in *Pik3ca*^{H1047R} model mammary tumors. A, normal mammary ducts (left) express K14 and K8. Glandular regions of ASC (middle) or AME (right) from R26-Pik3ca^{H1047R};MMTV-Cre^{NLST} mice. B, spindle cell tumor (left) and PDA (middle right) from p53$^{f/+}$;MMTV-Cre^{NLST} mice. C, glandular region of ASC (left), spindle cell tumor (middle), and PDA (right) from R26-Pik3ca^{H1047R};p53$^{f/+}$;MMTV-Cre^{NLST} mice. D, immunohistochemistry for ERα in R26-Pik3ca^{H1047R};MMTV-Cre^{NLST} ASCs (top left, top middle) and AMEs (top right) compared with normal mammary epithelium (inset). Western blot analysis for ERα (bottom left). Western signals were quantified as described earlier (bottom right). Bars, sample mean; error bars: ±SE; asterisks, significant increase (1-sided 1-sample *t* test; $\alpha = 0.05$; *, $P < 0.05$ and **, $P < 0.1$). White scale bars, 40 μm; black scale bars, 20 μm. Yellow dashed line, protein expression in a normal mammary gland.

Published OnlineFirst February 15, 2011; DOI: 10.1158/0008-5472.CAN-10-0738

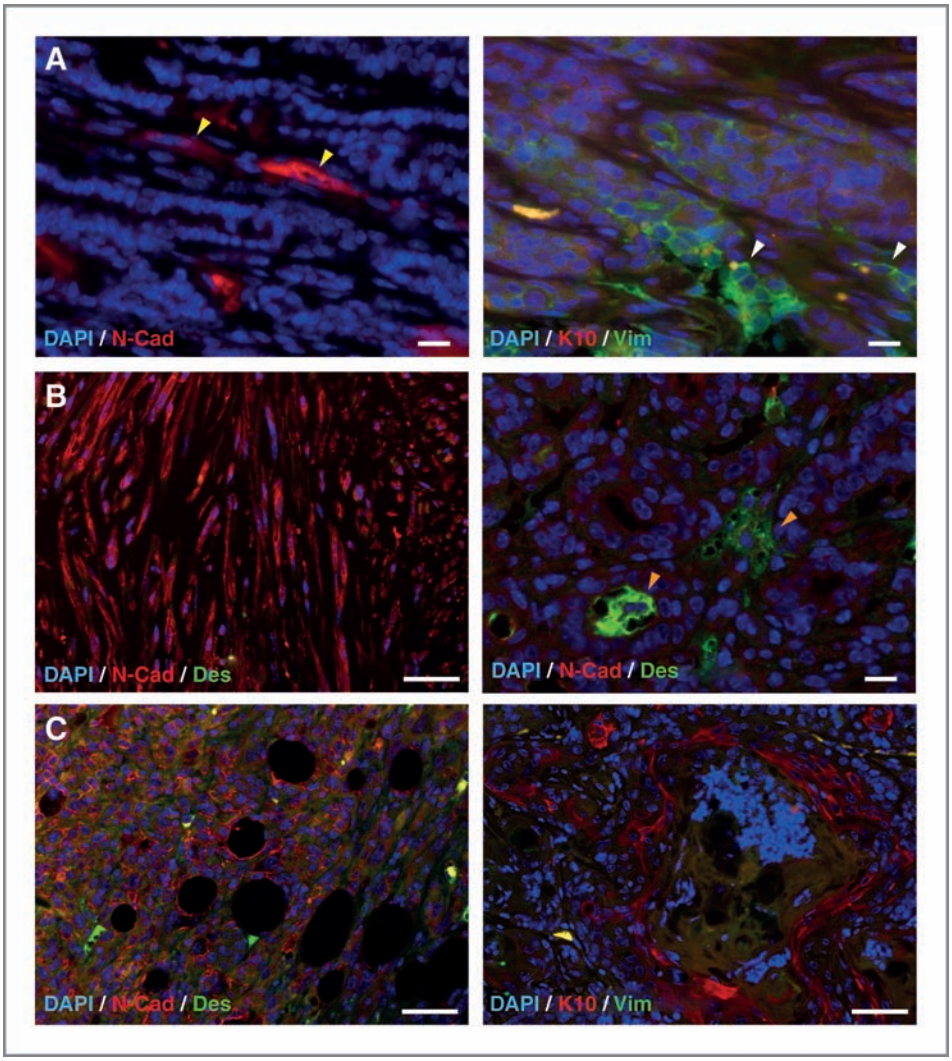

Figure 6. EMT in mammary tumors from *Pik3ca*^{H1047R} model mice. A, R26-Pik3ca^{H1047R}; MMTV-Cre^{NLST} adenosquamous carcinomas express N-Cad (left) and Vim (right). B, R26-Pik3ca^{H1047R};MMTV-Cre^{NLST} adenomyoepitheliomas express N-Cad (left) and Des (right). C, spindle tumors express N-Cad (left); adenosquamous carcinomas express K10 (right). Scale bars, 40 μm.

5 distinct types of mammary tumors in our *PIK3CA* model: adenosquamous carcinoma, adenomyoepithelialomas, spindle/EMT tumors, poorly differentiated adenocarcinomas, and radial scar type lesions. Although some of these tumor types are quite rare in humans, poorly differentiated adenocarcinomas are common, as are spindle/EMT tumors (Basal B tumors in humans). In addition, adenosquamous carcinomas are metaplastic, a tumor type in humans with a high frequency of *PIK3CA* mutations (11). This result is consistent with the wide spectrum of human breast cancers found to have *PIK3CA* mutations. In addition, our diverse collection of tumors includes ERα^{+} tumors and TNT-type tumors. This result contrasts with tumor models using Neu, Wnt, Myc, or Polyoma middle T, each of which induce a very specific mammary tumor type in mice (43).

We tested for PI3K pathway activation in major mammary tumor types that developed in our *PIK3CA*^{H1047R} model mice. To this end we analyzed Akt phosphorylation, which was elevated in each tumor type. The modest level of Akt activation noted was somewhat surprising, although this was related to the use of whole mammary gland control tissue rather than lin^{-} mammary epithelium for normalization (Supplementary Fig. 5). In any case, Akt-independent transformation has been noted in some breast tumors with a *PIK3CA* mutation (32), and other PDK1 substrates are thought to play a role in this case. Indeed, transgenic mice expressing activated alleles of *Akt1* from the MMTV LTR do not form mammary tumors, highlighting the importance of other PI3K pathways in breast cancer (44, 45). Future studies will be required to define the importance of specific PIP_3-responsive kinases and pathways in our *Pik3ca*^{H1047R} model.

By using the Cre-conditional knock-in system, we can compare mammary tumor formation in response to distinct alleles of *Pik3ca*, each expressed at precisely the same level and in the same cell types. For example, we can now directly compare mammary tumors in our R26-Pik3ca^{H1047R} model with tumor formation in mice expressing helical domain mutants of *Pik3ca*. As our system is Cre-inducible, we can

Published OnlineFirst February 15, 2011; DOI: 10.1158/0008-5472.CAN-10-0738

Table 1. Ki67 and TUNEL data for R26-Pik3ca^{H1047R};p53^{f};MMTV-Cre^{NLST} mouse mammary tumors

	TUNEL staining		Ki67 immunohistochemistry	
	Number of tumors	Positive cells (%)	Number of tumors	Positive cells (%)
Genotype and tumor type				
R26-Pik3ca^{H1047R};MMTV-Cre^{NLST}, ASC	4	0.27	6	23.7
p53$^{f/+}$;MMTV-Cre^{NLST}, PDA	2	0.26	4	1.9
p53$^{f/+}$;MMTV-Cre^{NLST}, Spindle	1	0.06	2	7.0
R26-Pik3ca^{H1047R};p53$^{f/+}$;MMTV-Cre^{NLST}, ASC	2	0.18	2	28.0
R26-Pik3ca^{H1047R};p53$^{f/+}$;MMTV-Cre^{NLST}, PDA	1	0.51	1	8.7
R26-Pik3ca^{H1047R};p53$^{f/+}$;MMTV-Cre^{NLST}, Spindle/EMT	2	0.15	6	12.6
Total	12		21	
Genotype				
R26-Pik3ca^{H1047R};MMTV-Cre^{NLST}	4	0.27	6	23.7
p53$^{f/+}$;MMTV-Cre^{NLST}	3	0.19	6	3.6
R26-Pik3ca^{H1047R};p53$^{f/+}$;MMTV-Cre^{NLST}	5	0.23	9	15.6
Total	12		21	
Tumor type				
ASC	6	0.24	8	24.8
PDA	3	0.34	5	3.3
Spindle/EMT	3	0.12	8	11.2
Total	12		21	

also compare mammary tumor formation in R26-Pik3ca^{H1047R};MMTV-Cre^{NLST} mice and in Pten$^{f/f}$;MMTV-Cre^{NLST} mice, in which PI3K pathway activation will occur in the same cell of origin but through a distinct mechanism. The importance of cell of origin can now be probed in our system as transgenic mice are available to activate *Pik3ca* alleles in luminal committed cells (WAP-Cre) and in bipotential cells expressing cytokeratin 14 (K14-Cre). Finally, this model can be used to identify genetic and cellular events associated with progression/metastasis, to screen for novel therapeutic targets in *Pik3ca^{H1047R}* mammary tumor cells *ex vivo* and to develop preclinical data on PI3K pathway inhibitors for treatment of breast cancer.

Disclosure of Potential Conflicts of Interest

No potential conflicts of interest were disclosed.

Acknowledgments

We thank Neil Adams, Farrah Awan, Adrian Cozma, Zhe Jiang, Tao Deng, Hui Qin Li, Jodi Garner, Marina Gertsenstein, Alex Manno, Molly Ruggeri, Brenda Cohen, and Aaron Kucharczuk for advice and/or technical support; Drs. C-C. Hui, Andras Nagy, Janet Rossant, and Brian Ciruna for advice/reagents; and Dr. Jean Andrey for statistical advice. Finally, we thank Dr. Robert Cardiff for comments on mouse tumor pathology.

Grant Support

We thank Restracomp from the Hospital for Sick Children for J.R. Adam's studentship and the Canadian Breast Cancer Foundation for funding of J.C. Liu. We thank the Komen Foundation for the Cure for funding to S.E. Egan and E. Zacksenhaus and the Canadian Breast Cancer Research Foundation—Ontario Division and Genome Canada for funding to S.E. Egan and the Canadian Breast Cancer Alliance for funding to E. Zacksenhaus.

The costs of publication of this article were defrayed in part by the payment of page charges. This article must therefore be hereby marked *advertisement* in accordance with 18 U.S.C. Section 1734 solely to indicate this fact.

Received March 2, 2010; revised November 5, 2010; accepted January 25, 2011; published OnlineFirst February 15, 2011.

References

1. Samuels Y, Wang Z, Bardelli A, Silliman N, Ptak J, Szabo S, et al. High frequency of mutations of the PIK3CA gene in human cancers. Science 2004;304:554.
2. Yuan TL, Cantley LC. PI3K pathway alterations in cancer: variations on a theme. Oncogene 2008;27:5497–510.
3. Wood LD, Parsons DW, Jones S, Lin J, Sjöblom T, Leary RJ, et al. The genomic landscapes of human breast and colorectal cancers. Science 2007;318:1108–13.
4. Saal LH, Holm K, Maurer M, Memeo L, Su T, Wang X, et al. PIK3CA mutations correlate with hormone receptors, node metastasis, and ERBB2, and are mutually exclusive with PTEN loss in human breast carcinoma. Cancer Res 2005;65:2554–9.
5. Bachman KE, Argani P, Samuels Y, Silliman N, Ptak J, Szabo S, et al. The PIK3CA gene is mutated with high frequency in human breast cancers. Cancer Biol Ther 2004;3:772–5.

Published OnlineFirst February 15, 2011; DOI: 10.1158/0008-5472.CAN-10-0738

6. Campbell IG, Russell SE, Choong DY, Montgomery KG, Ciavarella ML, Hooi CS, et al. Mutation of the PIK3CA gene in ovarian and breast cancer. Cancer Res 2004;64:7678–81.
7. Lee JW, Soung YH, Kim SY, Lee HW, Park WS, Nam SW, et al. PIK3CA gene is frequently mutated in breast carcinomas and hepatocellular carcinomas. Oncogene 2005;24:1477–80.
8. Li H, Zhu R, Wang L, Zhu T, Li Q, Chen Q, et al. PIK3CA mutations mostly begin to develop in ductal carcinoma of the breast. Exp Mol Pathol 2009;88:150–5.
9. Miron A, Varadi M, Carrasco D, Li H, Luongo L, Kim HJ, et al. PIK3CA mutations in in situ and invasive breast carcinomas. Cancer Res 2010;70:5674–8.
10. Dunlap J, Le C, Shukla A, Patterson J, Presnell A, Heinrich MC, et al. Phosphatidylinositol-3-kinase and AKT1 mutations occur early in breast carcinoma. Breast Cancer Res Treat 2010;120:409–18.
11. Hennessy BT, Gonzalez-Angulo AM, Stemke-Hale K, Gilcrease MZ, Krishnamurthy S, Lee JS, et al. Characterization of a naturally occurring breast cancer subset enriched in epithelial-to-mesenchymal transition and stem cell characteristics. Cancer Res 2009;69:4116–24.
12. Kim JS, Lee C, Bonifant CL, Ressom H, Waldman T. Activation of p53-dependent growth suppression in human cells by mutations in PTEN or PIK3CA. Mol Cell Biol 2007;27:662–77.
13. Buttitta F, Felicioni L, Barassi F, Martella C, Paolizzi D, Fresu G, et al. PIK3CA mutation and histological type in breast carcinoma: high frequency of mutations in lobular carcinoma. J Pathol 2006;208:350–5.
14. Maruyama N, Miyoshi Y, Taguchi T, Tamaki Y, Monden M, Noguchi S. Clinicopathologic analysis of breast cancers with PIK3CA mutations in Japanese women. Clin Cancer Res 2007;13:408–14.
15. Carson JD, Van Aller G, Lehr R, Sinnamon RH, Kirkpatrick RB, Auger KR, et al. Effects of oncogenic p110alpha subunit mutations on the lipid kinase activity of phosphoinositide 3-kinase. Biochem J 2008;409:519–24.
16. Mandelker D, Gabelli SB, Schmidt-Kittler O, Zhu J, Cheong I, Huang CH, et al. A frequent kinase domain mutation that changes the interaction between PI3Kalpha and the membrane. Proc Natl Acad Sci U S A 2009;106:16996–7001.
17. Huang CH, Mandelker D, Schmidt-Kittler O, Samuels Y, Velculescu VE, Kinzler KW, et al. The structure of a human p110alpha/p85alpha complex elucidates the effects of oncogenic PI3Kalpha mutations. Science 2007;318:1744–8.
18. Kang S, Bader AG, Vogt PK. Phosphatidylinositol 3-kinase mutations identified in human cancer are oncogenic. Proc Natl Acad Sci U S A 2005;102:802–7.
19. Zhao JJ, Liu Z, Wang L, Shin E, Loda MF, Roberts TM. The oncogenic properties of mutant p110alpha and p110beta phosphatidylinositol 3-kinases in human mammary epithelial cells. Proc Natl Acad Sci U S A 2005;102:18443–8.
20. Isakoff SJ, Engelman JA, Irie HY, Luo J, Brachmann SM, Pearline RV, et al. Breast cancer-associated PIK3CA mutations are oncogenic in mammary epithelial cells. Cancer Res 2005;65:10992–1000.
21. Srinivas S, Watanabe T, Lin CS, William CM, Tanabe Y, Jessell TM, et al. Cre reporter strains produced by targeted insertion of EYFP and ECFP into the ROSA26 locus. BMC Dev Biol 2001;1:4.
22. Soriano P. Generalized lacZ expression with the ROSA26 Cre reporter strain. Nat Genet 1999;21:70–1.
23. Schaft J, Ashery-Padan R, Van Der Hoeven F, Gruss P, Stewart AF. Efficient FLP recombination in mouse ES cells and oocytes. Genesis 2001;31:6–10.
24. Jonkers J, Meuwissen R, Van Der Gulden H, Peterse H, Van Der Valk M, Berns A. Synergistic tumor suppressor activity of BRCA2 and p53 in a conditional mouse model for breast cancer. Nat Genet 2001;29:418–25.
25. Wagner KU, Wall RJ, St-Onge L, Gruss P, Wynshaw-Boris A, Garrett L, et al. Cre-mediated gene deletion in the mammary gland. Nucleic Acids Res 1997;25:4323–30.
26. Li G, Robinson GW, Lesche R, Martinez-Diaz H, Jiang Z, Rozengurt N, et al. Conditional loss of PTEN leads to precocious development and neoplasia in the mammary gland. Development 2002;129:4159–70.
27. Jiang Z, Deng T, Jones R, Li H, Herschkowitz JI, Liu JC, et al. Rb deletion in mouse mammary progenitors induces luminal-B or basal-like/EMT tumor subtypes depending on p53 status. J Clin Invest 2010;120:3296–309.
28. Krymskaya VP, Goncharova EA. PI3K/mTORC1 activation in hamartoma syndromes: therapeutic prospects. Cell Cycle 2009;8:403–13.
29. Lin SC, Lee KF, Nikitin AY, Hilsenbeck SG, Cardiff RD, Li A, et al. Somatic mutation of p53 leads to estrogen receptor alpha-positive and -negative mouse mammary tumors with high frequency of metastasis. Cancer Res 2004;64:3525–32.
30. Cardiff RD. The pathology of EMT in mouse mammary tumorigenesis. J Mammary Gland Biol Neoplasia 2010;15:225–33.
31. Damonte P, Gregg JP, Borowsky AD, Keister BA, Cardiff RD. EMT tumorigenesis in the mouse mammary gland. Lab Invest 2007;87:1218–26.
32. Vasudevan KM, Barbie DA, Davies MA, Rabinovsky R, McNear CJ, Kim JJ, et al. AKT-independent signaling downstream of oncogenic PIK3CA mutations in human cancer. Cancer Cell 2009;16:21–32.
33. Birle D, Bottini N, Williams S, Huynh H, deBelle I, Adamson E, et al. Negative feedback regulation of the tumor suppressor PTEN by phosphoinositide-induced serine phosphorylation. J Immunol 2002;169:286–91.
34. Vivanco I, Palaskas N, Tran C, Finn SP, Getz G, Kennedy NJ, et al. Identification of the JNK signaling pathway as a functional target of the tumor suppressor PTEN. Cancer Cell 2007;11:555–69.
35. Kouros-Mehr H, Bechis SK, Slorach EM, Littlepage LE, Egeblad M, Ewald AJ, et al. GATA-3 links tumor differentiation and dissemination in a luminal breast cancer model. Cancer Cell 2008;13:141–52.
36. Kalluri R, Weinberg RA. The basics of epithelial-mesenchymal transition. J Clin Invest 2009;119:1420–8.
37. Zavadil J, Haley J, Kalluri R, Muthuswamy SK, Thompson E. Epithelial-mesenchymal transition. Cancer Res 2008;68:9574–7.
38. Wu X, Nguyen BC, Dziunycz P, Chang S, Brooks Y, Lefort K, et al. Opposing roles for calcineurin and ATF3 in squamous skin cancer. Nature 2010;465:368–72.
39. Kaluz S, Kaluzova M, Liao SY, Lerman M, Stanbridge EJ. Transcriptional control of the tumor- and hypoxia-marker carbonic anhydrase 9: A one transcription factor (HIF-1) show? Biochim Biophys Acta 2009;1795:162–72.
40. Wu G, Xing M, Mambo E, Huang X, Liu J, Guo Z, et al. Somatic mutation and gain of copy number of PIK3CA in human breast cancer. Breast Cancer Res 2005;7:R609–16.
41. Kadota M, Sato M, Duncan B, Ooshima A, Yang HH, Diaz-Meyer N, et al. Identification of novel gene amplifications in breast cancer and coexistence of gene amplification with an activating mutation of PIK3CA. Cancer Res 2009;69:7357–65.
42. Renner O, Blanco-Aparicio C, Grassow M, Canamero M, Leal JF, Carnero A. Activation of phosphatidylinositol 3-kinase by membrane localization of p110alpha predisposes mammary glands to neoplastic transformation. Cancer Res 2008;68:9643–53.
43. Herschkowitz JI, Simin K, Weigman VJ, Mikaelian I, Usary J, Hu Z, et al. Identification of conserved gene expression features between murine mammary carcinoma models and human breast tumors. Genome Biol 2007;8:R76.
44. Hutchinson J, Jin J, Cardiff RD, Woodgett JR, Muller WJ. Activation of Akt (protein kinase B) in mammary epithelium provides a critical cell survival signal required for tumor progression. Mol Cell Biol 2001;21:2203–12.
45. Schwertfeger KL, Richert MM, Anderson SM. Mammary gland involution is delayed by activated Akt in transgenic mice. Mol Endocrinol 2001;15:867–81.

Cancer Research
The Journal of Cancer Research (1916–1930) | The American Journal of Cancer (1931–1940)

AACR American Association for Cancer Research

Cooperation between *Pik3ca* and p53 Mutations in Mouse Mammary Tumor Formation

Jessica R. Adams, Keli Xu, Jeff C. Liu, et al.

Cancer Res 2011;71:2706-2717. Published OnlineFirst February 15, 2011.